

FastCar: Cache Attentive Replay for Fast Auto-Regressive Video Generation on the Edge

Xuan Shen^{1*}, Weize Ma^{2*}, Yufa Zhou³, Enhao Tang², Yanyue Xie¹, Zhengang Li⁴,
Yifan Gong⁴, Quanyi Wang⁵, Henghui Ding⁶, Yiwei Wang⁷,
Yanzhi Wang^{1†}, Pu Zhao^{1†}, Jun Lin^{2†}, Jiuxiang Gu^{4†}
¹Northeastern University, ²Nanjing University, ³Duke University,
⁴Adobe Research ⁵NUIST, ⁶Fudan University, ⁷UCM
shen.xu@northeastern.edu

Abstract

Auto-regressive (AR) models, initially successful in language generation, have recently shown promise in visual generation tasks due to their superior sampling efficiency. Unlike image generation, video generation requires a substantially larger number of tokens to produce coherent temporal frames, resulting in significant overhead during the decoding phase. Our key observations are: (i) MLP modules in the decode phase dominate the inference latency, and (ii) there exists high temporal redundancy in MLP outputs of adjacent frames. In this paper, we propose the **FastCar** framework to accelerate the decode phase for the AR video generation by exploring the temporal redundancy. The Temporal Attention Score (TAS) is proposed to determine whether to apply the replay strategy (*i.e.*, reusing cached MLP outputs from the previous frame to reduce redundant computations) with detailed theoretical analysis and justification. Also, we develop a hardware accelerator on FPGA with Dynamic Resource Scheduling (DRS) based on TAS to enable better resource utilization and faster inference. Experimental results demonstrate the effectiveness of our method, which outperforms traditional sparse attention approaches with more than $2.1\times$ decoding speedup and higher energy efficiency on the edge. Furthermore, by combining FastCar and sparse attention, FastCar can boost the performance of sparse attention with alleviated drifting, demonstrating our unique advantages for high-resolution and long-duration video generation. Code: <https://github.com/shawnricecake/fast-car>

1 Introduction

Recently, there has been growing interest in extending the Auto-Regressive (AR) framework of Large Language Models (LLMs) [1, 2, 3] to visual generation tasks [4, 5, 6, 7, 8, 9, 10, 11, 12, 13, 14, 15]. The works [4, 7, 12, 6, 15] convert images into tokens, and apply AR models to generate image tokens with next-token prediction. The generation quality is surprisingly strong, often rivaling or surpassing diffusion-based methods [7, 12, 6] in perceptual fidelity and semantic coherence.

As video becomes a dominant medium across entertainment, communication, *etc.*, synthesizing coherent high-quality videos from minimal inputs presents a compelling research challenge [16, 17, 18, 19]. Prior works [20, 21, 22, 23, 24, 25] leverage Diffusion Transformers (DiT) [26] to develop video generation models with superior generation performance, at the cost of substantial computations and massive memory demands [27, 28, 29, 30, 31]. These characteristics limit their applications and

*Equal Contribution

†Corresponding Authors

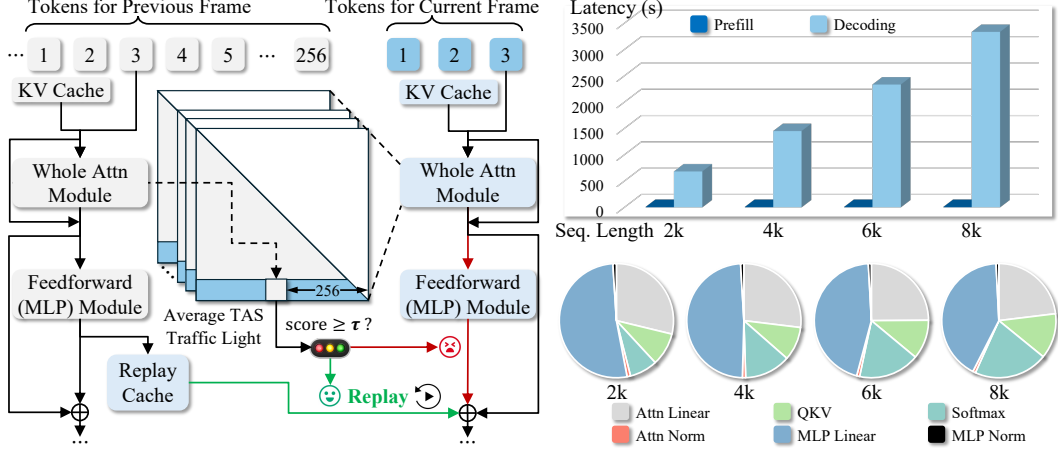


Figure 1: **Left:** FastCar framework. We replay the cache from the previous frame to skip the computations for MLP in decoding. Replay is triggered when the average TAS exceeds a predefined threshold τ . **Right Top:** Latency cost of both prefill and decode phases for different sequence lengths. **Right Bottom:** Detailed latency cost of the decode phase for different sequence lengths.

deployments for resource-constrained environments [32, 33, 34, 35, 36] such as mobile devices or Field-Programmable Gate Array (FPGA) with tight constraints for energy efficiency, memory, *etc.*

Motivated by the scalability and fast decoding capabilities of AR transformer-based frameworks in generative tasks, an increasing number of works [37, 9, 8, 11, 14] have adopted AR frameworks for video generation tasks. To further improve its efficiency, model compression strategies (such as pruning and quantization [38, 39, 40, 41, 42]) and spatial redundancy optimizations (such as sparse attention [43, 44, 45, 46, 47, 48] and efficient sampling methods [49, 50, 51, 52, 53, 54, 27, 31]) are investigated. However, the inherent temporal redundancy specifically introduced by videos with multiple sequential frames remains largely unexplored in AR video generation.

Specific Deep Insights. To explore the redundancy for superior efficiency, we first perform a detailed latency profiling and a similarity analysis between different frames. As shown in the right of Figure 1, we identify that the MLP modules (rather than the attention modules) in the decode phase dominate the inference latency. Meanwhile, according to Figure 2, the outputs of adjacent frames for the same MLP module exhibit relatively high resemblance/similarity, indicating high temporal redundancy.

Framework with Theoretical Justification. Based on the deep insights specific for AR video generation, we propose **FastCar** for efficiency optimization. We propose the *Temporal Attention Score (TAS)* to determine whether to skip the computations of the MLP modules. If skipped, the cached outputs from the previous frame are directly reused as current outputs (similar to video replay) due to their high similarity. Skipping the computation-intensive MLP modules leads to substantial accelerations. We further provide a detailed theoretical analysis to formally characterize how our TAS controls the output differences across adjacent frames, thereby justifying the design of FastCar.

Hardware Accelerator. We develop a flexible and efficiency-oriented hardware accelerator that supports kernel fusion and custom instruction programmability to allow direct reuse of cached outputs and enable conditional execution for MLP modules. To handle varying workload sparsity, we propose *Dynamic Resource Scheduling (DRS)*, which leverages attentivity to dynamically allocate computational resources. DRS, integrated into lightweight control logic, helps alleviate bandwidth pressure and improves overall resource efficiency, thereby enabling faster inference.

Comprehensive Experiments. Experimental results show that FastCar not only surpasses sparse attention (SA) methods with better generation quality, but also achieves faster decoding with improved energy efficiency on FPGA. Additionally, FastCar complements SA approaches by mitigating their drifting issues. By combining FastCar and SA, FastCar significantly boosts the generation quality of SA with faster inference and better long-range temporal coherence.

Our contributions are summarized as follows,

1. We perform the latency profiling and similarity analysis between different frames to explore the temporal redundancy in MLP modules. We then propose FastCar framework to accelerate AR video generation by replaying MLP modules using cached outputs from the previous frame.
2. Our theoretical analysis demonstrates that the similarity of MLP outputs across adjacent frames correlates with the attentivity, and this correlation is consistent across various model depths, thus justifying the design of FastCar with TAS (*i.e.*, the attentivity) to guide replay decisions.
3. We develop an efficiency-oriented hardware accelerator with DRS, enabling dynamic allocation of computational resources to enhance resource utilization and accelerate inference on FPGA.
4. Experimental results show that FastCar outperforms SA methods in generation quality and achieves more than $2.1\times$ speedup, while also alleviating drifting issues of SA methods, thereby enhancing scalability and efficiency for high-resolution and long-duration AR video generation.

2 Related Work

Auto-Regressive Visual Generation. Prior works [4, 5, 6, 7, 10, 11, 12, 13] apply the AR framework for image generation, demonstrating its potential to outperform diffusion-based models. In particular, VAR [7] introduces next-scale prediction to progressively generate token sequences across multiple resolutions, demonstrating the effectiveness of AR methods with enhanced image quality. Inspired by this, several works [37, 9, 8, 14] adopt the AR framework to develop video generation models. However, NOVA [9] and ART-V [8] still incorporate diffusion modules in their pipelines to boost generation quality, at the cost of substantially slower inference. Moreover, both models operate at the frame level rather than the token level, differing from the fine-grained, token-wise AR paradigm commonly used in LLMs. Unlike the above works, VILA-U [37] adopts the same AR framework as LLMs, making it one of the most promising approaches in video generation.

Efficient Techniques for Auto-Regressive Visual Generation. AR image generation models [4, 5], typically require n^2 sequential forward passes to generate an image represented by $n \times n$ tokens, resulting in significant inefficiency, which is further exacerbated when extending to video generation [37] with multiple image frames. Works [31, 54] accelerate the sampling process at decode phase, utilizing contextual cues from neighboring tokens to reduce redundant computations. The work [15] trains the model from scratch to enable parallel generation of adjacent token subsets for acceleration. However, this approach compromises global attention modeling, which limits the generation quality. The work [27] retains a short token sequence by incorporating neighboring tokens to enable efficient generation, thus reducing spatial redundancy. However, these works mainly investigate spatial redundancy, leaving the temporal redundancy of video generation largely unexplored.

3 Deep Insights for Auto-Regressive Video Generation

To effectively accelerate AR video generation, we first perform detailed profiling for the inference latency and computations of VILA-U [37]. We then provide the following specific deep insights: (i) The decode phase takes significantly longer than the prefill phase. (ii) The MLP modules dominate the latency of the decode phase. (iii) The outputs of an MLP module exhibit great similarity to those of its previous frame. Next we demonstrate our detailed observations and comprehensive analysis.

Prefill Phase v.s. Decode Phase. We compare the latency of the prefill phase and decode phase under different input sequence lengths from 2k to 8k, during AR video generation. As shown in the right top of Figure 1, the decode phase takes significantly longer than the prefill phase under various input lengths, as it needs to generate a large number of visual tokens for videos with multiple frames.

Attention Modules v.s. MLP Modules. We further explore detailed latency profiling for different decoding modules. The bottom right of Figure 1 shows that under varying input sequence lengths, MLP modules consistently dominate the overall latency. This observation underscores the distinct computational characteristics of AR generation compared with diffusion-based methods. Specifically, in diffusion transformers, all visual tokens are processed simultaneously through iterative denoising, with attention modules as the primary computational bottleneck. In contrast, AR models generate tokens sequentially, where attention modules only contribute marginally to the overall latency. As a result, efficiency-oriented techniques designed for attention modules are less effective in AR.

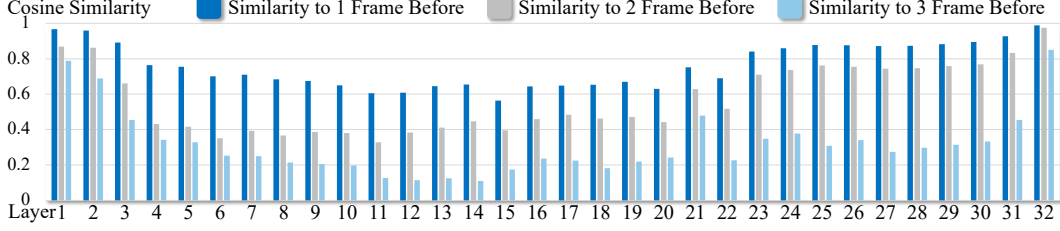


Figure 2: Cosine similarity for MLP outputs between neighboring frames for all 32 MLP modules.

Spatial Redundancy v.s. Temporal Redundancy. Spatial Redundancy is commonly explored in image generation with SA mechanisms (to reduce computations) or efficient sampling (to generate fewer tokens). In contrast, temporal redundancy in video generation remains largely overlooked, as prior works focus on image generation. To explore temporal redundancy, we present cosine similarity between outputs of an MLP module and those of its neighboring frames in Figure 2. The MLP outputs exhibit high similarity with their most recent frame, demonstrating high temporal redundancy.

Motivation. Based on the observation that MLP modules dominate the overall latency, we mainly optimize the computations of MLP modules for acceleration. The temporal redundancy with high similarities between the MLP outputs of neighboring frames further motivate us to cache the corresponding hidden states from the current time step for reuse in its next time step, thus avoiding its computations.

4 FastCar Framework Design

We demonstrate our FastCar framework in this section. In general, when the proposed *Temporal Attention Score (TAS)* indicates high similarity, we then directly reuse the cached outputs from its previous frame as the outputs of the current frame, thus skipping the MLP computations.

We first provide specific definitions for AR video generation. Then we demonstrate FastCar in great details. Theoretical analysis are further provided for the rationality and justification of FastCar.

4.1 Auto-Regressive Video Generation

We model a video \mathcal{V} as a temporal sequence of T frames with N visual tokens in each frame. With \mathcal{V}_{vis} denoting a finite vocabulary of visual tokens, it can be formulated as follows,

$$\mathcal{V} = \{z_{t,i} \mid t = 1, \dots, T; i = 1, \dots, N\}, \quad z_{t,i} \in \mathcal{V}_{\text{vis}}, \quad (1)$$

Flattening the temporal-spatial grid yields a sequence of length $n = T \cdot N$. We denote the flattened token index as $j = (t, i) := (t-1)N + i$, where t denotes the frame index and i denotes the index of the spatial position. Since frames are consecutively ordered, it satisfies: $(t-1, i) = (t, i) - N$.

For transformer layers, we define the hidden states: $X \in \mathbb{R}^{n \times d}$, where d denotes the hidden size. We use a batch size of $B = 1$ for simplicity, with all results readily extendable to $B > 1$ through broadcasting. The objective of AR video generation is to model the joint distribution:

$$P(\mathcal{V}) = \prod_{j=1}^n P(z_j \mid z_{<j}), \quad (2)$$

4.2 Key Modules

We now formalize the key modules in AR video generation and our FastCar framework. The model has multiple blocks, with an attention module and an MLP module for each block, as defined below.

Definition 4.1 (Attention Module). *Given hidden states $X \in \mathbb{R}^{n \times d}$, attention output is computed as:*

$$\text{Attn}(X) = \text{Softmax}\left(\frac{QK^\top}{\sqrt{d}}\right)V \in \mathbb{R}^{n \times d}, \text{ with } Q = XW_Q, K = XW_K, V = XW_V, \quad (3)$$

where $W_Q, W_K, W_V \in \mathbb{R}^{d \times d}$ are the query, key, and value projection matrices.

Definition 4.2 (MLP Module). Given input hidden states $X \in \mathbb{R}^{n \times d}$, the MLP module is defined as:

$$\text{MLP}(X) = (\text{act}(XW_G) \circ (XW_U)) W_D \in \mathbb{R}^{n \times d}, \quad (4)$$

where $\text{act}(\cdot)$ is a non-linear activation function (e.g., SiLU), \circ denotes element-wise multiplication, and $W_G, W_U \in \mathbb{R}^{d \times d_{\text{ff}}}$, $W_D \in \mathbb{R}^{d_{\text{ff}} \times d}$ are learned parameters with the intermediate size of d_{ff} .

Next we define TAS to measure the token similarity of adjacent frames and guide replay decisions.

Definition 4.3 (Temporal Attention Score). The temporal attention score at spatial position i and t -th frame is defined as the scaled dot-product between the query vector q_j of token $j = (t, i)$ and the key vector k_{j^-} of its aligned token $j^- = (t-1, i)$:

$$s_{t,i} = \frac{\langle q_j, k_{j^-} \rangle}{\sqrt{d}} \in \mathbb{R}. \quad (5)$$

In our FastCar framework, due to causal decoding, TAS is obtained directly from the attention module preceding the MLP, thus there is no additional computation cost.

4.3 Cache Attentive Replay for Fast Generation (FastCar)

In FastCar, with TAS, we enable attentive replay in MLP modules by manually setting a threshold τ to filter tokens of adjacent frames with higher attentivity. When TAS is larger than τ , which indicates significant temporal similarity, we skip MLP computations by reusing the outputs of its previous frame at the same spatial location.

Specifically, for each transformer block, at frame $t - 1$, for each spatial token index i , we cache the MLP output as follows:

$$Y_{(t-1,i),:} = \text{MLP}(\text{Attn}(X) + X)_{(t-1,i),:}. \quad (6)$$

At frame t , we evaluate the set of TAS $\{s_{t,i}^{(m)}\}_{m=1}^h$ between token (t, i) and its aligned token $(t-1, i)$ across all h attention heads (Definition 4.3), and compute the mean score:

$$\bar{s}_{t,i} = \frac{1}{h} \sum_{m=1}^h s_{t,i}^{(m)}. \quad (7)$$

When the mean score exceeds a predefined threshold τ , i.e., $\bar{s}_{t,i} \geq \tau$, we then skip the following MLP computations of this specific token (t, i) and reuse the cached output for the replay in the block:

$$Y_{(t,i),:} = \begin{cases} Y_{(t-1,i),:}, & \text{if } \bar{s}_{t,i} \geq \tau \\ \text{MLP}(\text{Attn}(X) + X)_{(t,i),:}, & \text{Otherwise} \end{cases}. \quad (8)$$

Otherwise, we still perform the normal MLP computations. In the AR model, there are multiple transformer blocks with the same architecture following the same computation pattern. We apply FastCar for each block. This selective replay mechanism reduces MLP computations by leveraging temporal consistency across adjacent frames.

4.4 Theoretical Similarity Analysis

We now formally characterize how TAS controls the output differences across adjacent frames, thereby justifying temporal replay based on TAS.

We first relate temporal attention similarity to the difference in attention outputs.

Theorem 4.4 (Attention Score Controls Attention Output Difference). Let $X \in \mathbb{R}^{n \times d}$ be the hidden states, where each row $x_j \in \mathbb{R}^d$ represents the hidden state of token j . Let $\text{Attn}(X)$ denote the attention output defined in Definition 4.1. For tokens $j = (t, i)$ and $j^- = (t-1, i)$ aligned at the same spatial position, define the temporal attention score $s_{t,i}$ as in Definition 4.3. Assume that:

- (1) The hidden states are bounded: $\|x_j\|_2 \leq M$ for all j ;
- (2) The projection matrices satisfy $\|W_Q\|_2, \|W_K\|_2 \leq \Lambda$;
- (3) The query and key vectors are normalized: $\|q_j\|_2 = \|k_{j^-}\|_2 = 1$ for all j .

Let $\gamma := \|W_Q - W_K\|_2$ denote the projection difference.

Then, under the Lipschitz continuity of the attention, there exists a constant $C > 0$ such that:

$$\|\text{Attn}(X)_{j,:} - \text{Attn}(X)_{j^-,:}\|_2 \leq C \left(\sqrt{1 - s_{t,i}} + \gamma M \right). \quad (9)$$

Thus, a larger $s_{t,i}$ implies a smaller attention output difference up to a model-dependent offset γM .

In practice, transformers often apply normalization techniques (such as LayerNorm or explicit vector normalization) to control query and key magnitudes. Thus assuming $\|q_j\|_2 = \|k_{j^-}\|_2 = 1$ is reasonable and standard for theoretical analysis [36, 41]. We delay the full proof to Appendix 10.

Remark 4.5. The TAS $s_{t,i}$ depends only on the local query and key vectors at the current layer and is independent of model depth. It captures instantaneous similarity without accumulating information across layers, making it a stable, efficient, and fine-grained signal for dynamic computation reduction during auto-regressive decoding.

Next, we relate input and attention similarity to MLP output similarity.

Theorem 4.6 (Attention and Input Similarity Implies MLP Output Similarity). *Let $\text{MLP}(\cdot)$ denote the MLP module defined in Definition 4.2. Let $Y_{j,:} = \text{MLP}(\text{Attn}(X) + X)_{j,:}$ and $Y_{j^-,:} = \text{MLP}(\text{Attn}(X) + X)_{j^-,:}$ denote the MLP outputs at tokens j and j^- .*

Assume that $\text{MLP}(\cdot)$ is L -Lipschitz continuous. Then

$$\|Y_{j,:} - Y_{j^-,:}\|_2 \leq L (\|X_{j,:} - X_{j^-,:}\|_2 + \|\text{Attn}(X)_{j,:} - \text{Attn}(X)_{j^-,:}\|_2). \quad (10)$$

The proof is demonstrated in Appendix 10. Finally, combining the two results, we directly relate TAS to MLP output similarity.

Theorem 4.7 (Temporal Attention Score Controls MLP Output Similarity). *Let $X \in \mathbb{R}^{n \times d}$ be the hidden states, and let $Y_{j,:}$ and $Y_{j^-,:}$ denote the MLP outputs at tokens j and j^- . Let $s_{t,i}$ denote the temporal attention score. Under the assumptions of Theorem 4.4 and assuming the MLP is L -Lipschitz, there exists a constant $C > 0$ such that:*

$$\|Y_{j,:} - Y_{j^-,:}\|_2 \leq C (\|X_{j,:} - X_{j^-,:}\|_2 + \sqrt{1 - s_{t,i}} + \gamma M). \quad (11)$$

The proof is demonstrated in Appendix 10. Theorem 4.7 formally establishes that high TAS, combined with input similarity, guarantees small MLP output deviation across adjacent frames. This justifies the use of thresholds on TAS to dynamically skip MLP computations during decoding, enabling efficient temporal replay with controlled quality loss. Moreover, as TAS is computed layer-locally, it offers a stable and depth-independent signal for runtime adaptation (Remark 4.5).

5 Hardware Design

We develop a programmable hardware accelerator, as shown in the left of Figure 3. Pre-compiled instructions are loaded via the AXI bus with the Fetch module, and dispatched to the corresponding instruction FIFO (First-In-First-Out). The Control module manages the Matrix Unit (MU) and Vector Unit (VU) to perform matrix multiplication and vector computation, while the Direct Memory Access (DMA) module is responsible for loading data from off-chip memory (i.e., DDR or HBM). The instruction FIFO receives control signals from the Control Module to coordinate the computations of each unit. The Dynamic Resource Scheduling (DRS) module is employed to address the computational workload imbalance caused by dynamic replay from the FastCar framework.

Dynamic Resource Scheduling (DRS)

The FastCar framework dynamically determines whether to adopt the replay strategy to skip computations for certain MLP modules based on the TAS of different batches. Due to the multi-core design, computations for different batches in dense mode are mapped to distinct cores statically. However, the dynamic FastCar introduces computational workload imbalance across different cores, as the number of MLPS computed for different batches may vary and is difficult to predict during inference. Moreover, we employ static compilation to pre-generate scheduling instructions. Exhaustively enumerating all possible cases would incur an unaffordable large instruction storage overhead.

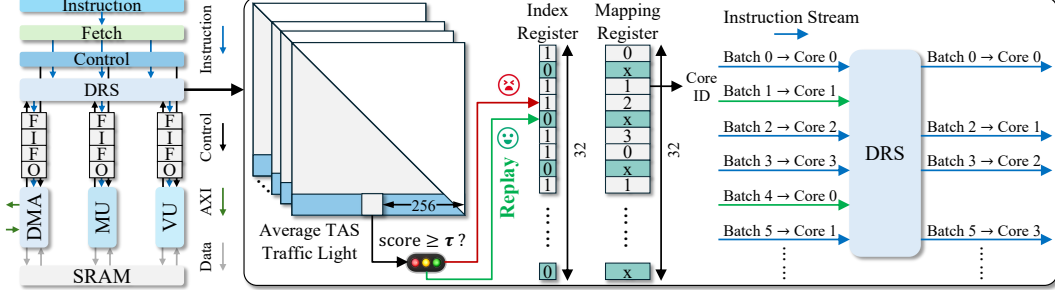


Figure 3: **Left:** The top-level block diagram of our hardware accelerator. **Right:** The DRS diagram.

To address this, we propose the DRS to balance the computational workloads, as shown in the right of Figure 3. After computing TAS, we configure an on-chip computation mapping table. A 32-bit Index Register, which stores the status of each batch (0=replay, 1=compute), is established to determine whether computation should be skipped. 32 Mapping Registers, each with $\log_2(\text{num_cores})$ bits, determine the target core for executing which batch. We adopt a round-robin assignment strategy to ensure balanced workload distribution among the cores.

When pre-compiled instructions are loaded and the replay mechanism is triggered, the prefetched instructions are forwarded to the DRS for processing. The DRS then performs scheduling decisions by consulting the Index Register to determine whether to discard instructions for replayed batches or dispatch them to the appropriate cores based on the Mapping Registers. Notably, the DRS incurs minimal overhead by completing its dispatch operations in just hundreds to thousands of cycles, which is negligible compared to the thousands of cycles required for actual instruction execution.

6 Experimental Results

6.1 Experimental Setup

In our experiments, we mainly adopt the AR video generation model from VILA-U [37] developed based on the LLaMA-2-7B [55] and RQ-VAE [56]. The quantizer codebook size is 16384. All videos are generated with 8 frames in 256×256 resolution, where each frame is decoded by 256 tokens. VILA-U is the only available open-source model in the novel research direction of AR video generation without diffusion. We evaluate the quality of generated videos with VBench [57], and the similarity of generated videos with metrics including Peak Signal-to-Noise Ratio (PSNR), Structural Similarity Index Measure (SSIM), and Learned Perceptual Image Patch Similarity (LPIPS) [58]. In detail, we compute the average similarity across all frames except the first one, as our method generates the first frame in the same manner as the baseline. We generate videos using prompts from VBench with a batch size of 5, a fixed random seed of 42, and classifier-free guidance of 3 [59] on A100 GPUs. Additionally, there are no available direct baselines in this novel area, and we mainly compare our method against the sparse attention (SA) approach StreamingLLM [43]. We set the sink size by extending the prefill length by 256 to ensure that attention to the first frame is preserved throughout video generation, thereby ensuring a fair comparison.

For hardware implementation, we adopt the Xilinx Alveo U280 FPGA as the target platform with a chiplet design. We implement multiple accelerator cores on the FPGA to ensure physical implementation feasibility. Latency and power are tested using a prefill sequence length of 256.

6.2 Main Results

We provide the main results with different replay ratios compared with the SA method in Table 1. The detailed VBench scores for all results in different dimensions are included in Appendix 8. We obtain the following observations: (i) The SA methods, such as StreamingLLM [43] are not able to accelerate AR video generation models effectively. When its local size shrinks with increasing sparsity, the computations measured by TFLOPs only decrease marginally without significant accelerations. The reason is that the MLP modules dominate the computations/latency, and thus optimizing attention modules does not effectively address the bottleneck. (ii) Our method effectively reduce

Table 1: Main results of the proposed method compared with the sparse attention based approach StreamingLLM [43], where dense attention is retained in the first frame for fair comparison. Local size denotes number of local tokens for sparse attention. Detailed VBench scores are in Appendix 8. Latency is tested for whole generation of one video. Power efficiency is computed by GFLOPs/W.

Method	Replay Ratio	Local Size	PSNR ↑	SSIM ↑	LPIPS ↓	VBench Score			TFLOPs ↓	Latency (s) ↓	Power Effi. ↑
						Total	Quality	Semantic			
Dense	/	/	-	-	-	74.1%	76.4%	65.0%	31.79	689.7 (1×)	1.47
Sparse Attn.	/	256	18.25	51.54	33.59	72.1%	74.6%	62.5%	30.95	670.5 (1.02×)	1.51
	/	128	13.14	33.61	54.34	60.7%	61.9%	55.9%	30.82	666.9 (1.03×)	1.52
	/	64	13.47	33.79	53.54	62.6%	63.3%	60.2%	30.76	666.3 (1.03×)	1.52
	/	32	13.34	33.14	53.82	61.4%	61.3%	62.0%	30.72	663.9 (1.04×)	1.52
	/	16	13.30	32.02	53.75	64.5%	64.8%	63.3%	30.70	662.7 (1.04×)	1.53
Ours	10%	/	18.57	53.32	27.31	73.4%	75.5%	65.2%	30.09	629.1 (1.10×)	1.61
	20%	/	17.94	51.01	27.57	73.2%	75.3%	65.1%	28.64	556.8 (1.24×)	1.82
	30%	/	17.87	50.29	28.02	72.4%	74.3%	64.7%	27.18	525.2 (1.31×)	1.93
	40%	/	17.68	50.14	28.15	71.8%	73.0%	67.2%	25.73	487.2 (1.42×)	2.08
	50%	/	17.85	50.11	28.08	71.5%	72.7%	66.6%	24.27	475.3 (1.45×)	2.13
	60%	/	17.85	50.55	28.72	71.4%	72.7%	66.2%	22.33	451.9 (1.53×)	2.24
	70%	/	17.86	50.18	28.79	71.2%	72.3%	66.9%	20.88	415.8 (1.66×)	2.43
	80%	/	17.71	49.01	29.50	71.5%	73.0%	65.6%	19.42	390.7 (1.76×)	2.59

the computations and achieve significant accelerations with better power efficiency. With an 80% replay ratio, our method can reduce 45% computations with a $1.77\times$ acceleration. (iii) Our method better maintains the generation quality than the SA methods. For similarity metrics including PSNR, SSIM, and LPIPS, with gradually increasing sparsity, our generation quality only degrades marginally, which is different from the significant performance losses of SA method. For the VBench scores, we can make similar observations. Specifically, when increasing the sparsity, unlike SA method with a significant drop on the total score (from 74.1% to 60.7%), our method consistently keeps a total score above 71.2% under various sparsity levels (even with an 80% replay ratio). Meanwhile, our method achieves higher power efficiency compared to the SA method, demonstrating strong potential for deployment in resource-constrained environments such as edge devices and mobile platforms. Furthermore, we provide the visualization with our method in different replay ratios in Appendix 9. The visualization shows that the video quality is well preserved across different replay ratios, and remains high even when the threshold τ is set to a very low value with a large replay ratio. To summarize, FastCar maintains better generation quality with larger accelerations than SA methods.

6.3 Ablation Study

Threshold Distributions. We conduct an ablation study on threshold distribution by applying either consistent or layer-wise varying (i.e., inconsistent) thresholds across all layers, while maintaining the same overall replay ratio. The ablation results are shown in the left side of Figure 4. We observe that consistent threshold achieves better performance with lower LPIPS and higher VBench score than inconsistent thresholds, which verifies the effectiveness of Remark 4.5 discussed in Section 4.4.

Threshold Values. Meanwhile, we ablate the threshold values to evaluate their impact on model performance, as shown in the right side of Figure 4. When $\tau \leq -2.5$, if we continue to decrease τ , the generation quality does not further degrade while higher sparsity with faster inference can be achieved, demonstrating the robustness of FastCar. Additionally, we observe that the AR video generation model achieves the highest replay ratio of 87% when $\tau \approx -8$, indicating that only 13% of the MLP modules are actually required during the generation process.

6.4 Additional Analysis

Replay Ratio Distribution. We visualize the replay ratio distribution across layers for 3 different thresholds in Figure 5. We observe that the model tends to replay at the shallow and deep layers, while replay is less likely to occur in intermediate layers. This indicates that intermediate layers play a critical role in capturing temporal dynamics and contribute most significantly to generation quality in auto-regressive video models.

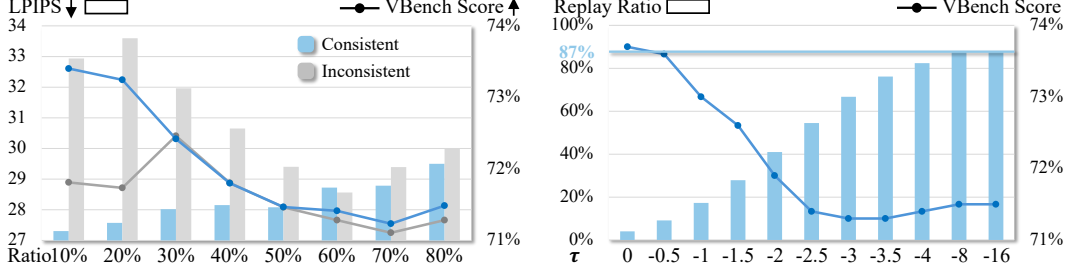


Figure 4: **Left:** Ablation study comparing consistent vs. inconsistent threshold settings with respect to LPIPS and the VBenCh total score. Full results are provided in Table 5 at Appendix 8. **Right:** Ablation study on the effect of the threshold τ on replay ratio and VBenCh total score. Full results are reported in Table 6 at Appendix 8.

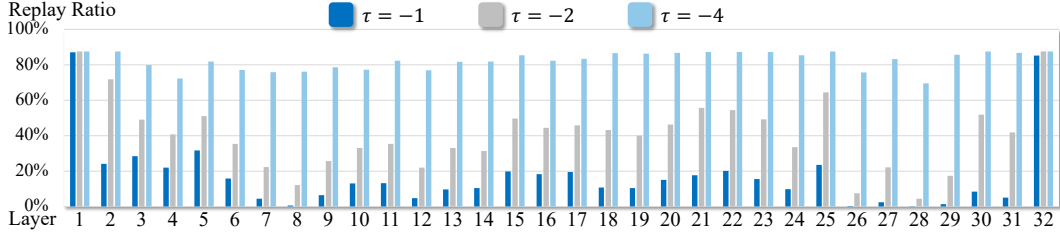


Figure 5: Replay ratio distribution across layers for thresholds $\tau = -1, -2$, and -4 , respectively.

Combination with Sparse Attention. We further provide additional results achieved by combining SA method and our method in Table 2. The detailed VBenCh scores for all results in different dimensions are included in Table 7 at Appendix 8. The results show that our method can significantly boost the performance of the SA method through a straightforward combination. This validates the effectiveness of our method as a complementary enhancement to existing SA approaches. We further visualize the results of our method, the SA approach, and their combination in Figure 6 to directly illustrate how our method alleviates drifting when integrated into sparse attention.

7 Conclusion

We propose FastCar, a framework to accelerate AR video generation on the edge. We show that the similarity across adjacent frames correlates with attentivity and is independent with model depths. We then introduce a replay strategy that reuses cached MLP outputs from the previous frame to reduce computation. Also, the DRS design is adopted to improve resource utilization and inference speed on FPGAs. Results show that our method outperforms prior SA approaches and complements them with more than $2.1\times$ speedup, enabling better scalability for high-resolution, long-duration video generation. In future work, we plan to extend our framework to a broader range of model families.

Table 2: Additional results for the combination of the sparse attention method and our method. More results are included in Table 7 at Appendix 8.

Method	Replay Ratio	Local Size	PSNR \uparrow	SSIM \uparrow	LPIPS \downarrow	VBenCh Score			GFLOPs \downarrow	Latency (s) \downarrow	Power Effi. \uparrow
						Total	Quality	Semantic			
Dense	/	/	-	-	-	74.1%	76.4%	65.0%	31.79	689.7 (1 \times)	1.47
Ours + Sparse Attn.	87%	256	17.44	47.57	31.27	71.8%	73.3%	65.7%	17.61	354.46 (1.95 \times)	2.85
	87%	128	17.29	46.79	32.10	71.7%	73.3%	65.7%	17.49	342.25 (2.02 \times)	2.96
	87%	64	17.27	46.70	32.09	71.6%	73.1%	65.5%	17.43	334.57 (2.06 \times)	3.02
	87%	32	17.27	46.75	31.96	71.9%	73.4%	65.9%	17.40	327.36 (2.11 \times)	3.09
	87%	16	17.27	46.49	32.37	71.6%	73.1%	65.7%	17.39	324.31 (2.13 \times)	3.12



Figure 6: Visualization for the prompt "A dog wearing sunglasses on the beach.". The second and third rows are generated with threshold $\tau = -4$ (i.e., 82% replay ratio). The third and fourth rows are generated with a sink size that extends the prompt length by one frame and 64.

References

- [1] Alec Radford, Jeff Wu, Rewon Child, David Luan, Dario Amodei, and Ilya Sutskever. Language models are unsupervised multitask learners. 2019.
- [2] Hugo Touvron, Thibaut Lavril, Gautier Izacard, Xavier Martinet, Marie-Anne Lachaux, Timothée Lacroix, Baptiste Rozière, Naman Goyal, Eric Hambro, Faisal Azhar, et al. Llama: Open and efficient foundation language models. *arXiv preprint arXiv:2302.13971*, 2023.
- [3] Aaron Grattafiori, Abhimanyu Dubey, Abhinav Jauhri, Abhinav Pandey, Abhishek Kadian, Ahmad Al-Dahle, Aiesha Letman, Akhil Mathur, Alan Schelten, Alex Vaughan, et al. The llama 3 herd of models. *arXiv preprint arXiv:2407.21783*, 2024.
- [4] Peize Sun, Yi Jiang, Shoufa Chen, Shilong Zhang, Bingyue Peng, Ping Luo, and Zehuan Yuan. Autoregressive model beats diffusion: Llama for scalable image generation. *arXiv preprint arXiv:2406.06525*, 2024.
- [5] Xinlong Wang, Xiaosong Zhang, Zhengxiong Luo, Quan Sun, Yufeng Cui, Jinsheng Wang, Fan Zhang, Yuezhe Wang, Zhen Li, Qiying Yu, et al. Emu3: Next-token prediction is all you need. *arXiv preprint arXiv:2409.18869*, 2024.
- [6] Jian Han, Jinlai Liu, Yi Jiang, Bin Yan, Yuqi Zhang, Zehuan Yuan, Bingyue Peng, and Xiaobing Liu. Infinity: Scaling bitwise autoregressive modeling for high-resolution image synthesis, 2024.
- [7] Keyu Tian, Yi Jiang, Zehuan Yuan, Bingyue Peng, and Liwei Wang. Visual autoregressive modeling: Scalable image generation via next-scale prediction. 2024.
- [8] Wenming Weng, Ruoyu Feng, Yanhui Wang, Qi Dai, Chunyu Wang, Dacheng Yin, Zhiyuan Zhao, Kai Qiu, Jianmin Bao, Yuhui Yuan, Chong Luo, Yueyi Zhang, and Zhiwei Xiong. Artv: Auto-regressive text-to-video generation with diffusion models. *arXiv preprint arXiv:2311.18834*, 2023.
- [9] Haoge Deng, Ting Pan, Haiwen Diao, Zhengxiong Luo, Yufeng Cui, Huchuan Lu, Shiguang Shan, Yonggang Qi, and Xinlong Wang. Autoregressive video generation without vector quantization. *arXiv preprint arXiv:2412.14169*, 2024.
- [10] Siyu Jiao, Gengwei Zhang, Yinlong Qian, Jiancheng Huang, Yao Zhao, Humphrey Shi, Lin Ma, Yunchao Wei, and Zequn Jie. Flexvar: Flexible visual autoregressive modeling without residual prediction. *arXiv preprint arXiv:2502.20313*, 2025.

- [11] Desai Xie, Zhan Xu, Yicong Hong, Hao Tan, Difan Liu, Feng Liu, Arie Kaufman, and Yang Zhou. Progressive autoregressive video diffusion models. *arXiv preprint arXiv:2410.08151*, 2024.
- [12] Peize Sun, Yi Jiang, Shoufa Chen, Shilong Zhang, Bingyue Peng, Ping Luo, and Zehuan Yuan. Autoregressive model beats diffusion: Llama for scalable image generation. *arXiv preprint arXiv:2406.06525*, 2024.
- [13] Zhuoyan Luo, Fengyuan Shi, Yixiao Ge, Yujiu Yang, Limin Wang, and Ying Shan. Openmagvit2: An open-source project toward democratizing auto-regressive visual generation. *arXiv preprint arXiv:2409.04410*, 2024.
- [14] Dan Kondratyuk, Lijun Yu, Xiuye Gu, José Lezama, Jonathan Huang, Grant Schindler, Rachel Hornung, Vighnesh Birodkar, Jimmy Yan, Ming-Chang Chiu, et al. Videopoet: A large language model for zero-shot video generation. *arXiv preprint arXiv:2312.14125*, 2023.
- [15] Yuqing Wang, Shuhuai Ren, Zhijie Lin, Yujin Han, Haoyuan Guo, Zhenheng Yang, Difan Zou, Jiashi Feng, and Xihui Liu. Parallelized autoregressive visual generation. *arXiv preprint arXiv:2412.15119*, 2024.
- [16] Jing Xiong, Gongye Liu, Lun Huang, Chengyue Wu, Taiqiang Wu, Yao Mu, Yuan Yao, Hui Shen, Zhongwei Wan, Jinfa Huang, et al. Autoregressive models in vision: A survey. *arXiv preprint arXiv:2411.05902*, 2024.
- [17] Zhen Xing, Qijun Feng, Haoran Chen, Qi Dai, Han Hu, Hang Xu, Zuxuan Wu, and Yu-Gang Jiang. A survey on video diffusion models. *ACM Computing Surveys*, 57(2):1–42, 2024.
- [18] Chengxuan Li, Di Huang, Zeyu Lu, Yang Xiao, Qingqi Pei, and Lei Bai. A survey on long video generation: Challenges, methods, and prospects. *arXiv preprint arXiv:2403.16407*, 2024.
- [19] Andrew Melnik, Michal Ljubljanac, Cong Lu, Qi Yan, Weiming Ren, and Helge Ritter. Video diffusion models: A survey. *Transactions on Machine Learning Research*, 2024. Survey Certification.
- [20] Bin Lin, Yunyang Ge, Xinhua Cheng, Zongjian Li, Bin Zhu, Shaodong Wang, Xianyi He, Yang Ye, Shenghai Yuan, Liuhan Chen, et al. Open-sora plan: Open-source large video generation model. *arXiv preprint arXiv:2412.00131*, 2024.
- [21] Zangwei Zheng, Xiangyu Peng, Tianji Yang, Chenhui Shen, Shenggui Li, Hongxin Liu, Yukun Zhou, Tianyi Li, and Yang You. Open-sora: Democratizing efficient video production for all. *arXiv preprint arXiv:2412.20404*, 2024.
- [22] Xiangyu Peng, Zangwei Zheng, Chenhui Shen, et al. Open-sora 2.0: Training a commercial-level video generation model in \$200k. *arXiv preprint arXiv:2503.09642*, 2025.
- [23] Wenyi Hong, Ming Ding, Wendi Zheng, Xinghan Liu, and Jie Tang. Cogvideo: Large-scale pretraining for text-to-video generation via transformers. *arXiv preprint arXiv:2205.15868*, 2022.
- [24] Zhuoyi Yang, Jiayan Teng, Wendi Zheng, Ming Ding, , et al. Cogvideox: Text-to-video diffusion models with an expert transformer. *arXiv preprint arXiv:2408.06072*, 2024.
- [25] Weijie Kong, Qi Tian, Zijian Zhang, Rox Min, Zuozhuo Dai, Jin Zhou, Jiangfeng Xiong, Xin Li, et al. Hunyuanvideo: A systematic framework for large video generative models, 2024.
- [26] William Peebles and Saining Xie. Scalable diffusion models with transformers. *arXiv preprint arXiv:2212.09748*, 2022.
- [27] Yefei He, Yuanyu He, Shaoxuan He, Feng Chen, Hong Zhou, Kaipeng Zhang, and Bohan Zhuang. Neighboring autoregressive modeling for efficient visual generation. *arXiv preprint arXiv:2503.10696*, 2025.
- [28] Yang Jin, Zhicheng Sun, Ningyuan Li, Kun Xu, Hao Jiang, Nan Zhuang, Quzhe Huang, Yang Song, Yadong Mu, and Zhouchen Lin. Pyramidal flow matching for efficient video generative modeling. *arXiv preprint arXiv:2410.05954*, 2024.

- [29] Ruyi Xu, Guangxuan Xiao, Haofeng Huang, Junxian Guo, and Song Han. Xattention: Block sparse attention with antidiagonal scoring. *arXiv preprint arXiv:2503.16428*, 2025.
- [30] Haocheng Xi, Shuo Yang, Yilong Zhao, Chenfeng Xu, Muyang Li, Xiuyu Li, Yujun Lin, Han Cai, Jintao Zhang, Dacheng Li, et al. Sparse videogen: Accelerating video diffusion transformers with spatial-temporal sparsity. *arXiv preprint arXiv:2502.01776*, 2025.
- [31] Yefei He, Feng Chen, Yuanyu He, Shaoxuan He, Hong Zhou, Kaipeng Zhang, and Bohan Zhuang. Zipar: Accelerating auto-regressive image generation through spatial locality. *arXiv preprint arXiv:2412.04062*, 2024.
- [32] Jun Liu, Shulin Zeng, Li Ding, Widyadewi Soedarmadji, Hao Zhou, Zehao Wang, Jinhao Li, Jintao Li, Yadong Dai, Kairui Wen, Shan He, Yaqi Sun, Yu Wang, and Guohao Dai. Flightvgm: Efficient video generation model inference with online sparsification and hybrid precision on fpgas. In *Proceedings of the 2025 ACM/SIGDA International Symposium on Field Programmable Gate Arrays, FPGA '25*, page 2–13, New York, NY, USA, 2025. Association for Computing Machinery.
- [33] Junchen Zhu, Huan Yang, Wenjing Wang, Huiguo He, Zixi Tuo, Yongsheng Yu, Wen-Huang Cheng, Lianli Gao, Jingkuan Song, Jianlong Fu, et al. Mobilevidfactory: Automatic diffusion-based social media video generation for mobile devices from text. In *Proceedings of the 31st ACM International Conference on Multimedia*, pages 9371–9373, 2023.
- [34] Bosung Kim, Kyuhwan Lee, Isu Jeong, Jungmin Cheon, Yeojin Lee, and Seulki Lee. On-device sora: Enabling diffusion-based text-to-video generation for mobile devices. *arXiv preprint arXiv:2502.04363*, 2025.
- [35] Xudong Lu, Aojun Zhou, Ziyi Lin, Qi Liu, Yuhui Xu, Renrui Zhang, Yafei Wen, Shuai Ren, Peng Gao, Junchi Yan, and Hongsheng Li. Terdit: Ternary diffusion models with transformers, 2024.
- [36] Xuan Shen, Zhao Song, Yufa Zhou, Bo Chen, Yanyu Li, Yifan Gong, Kai Zhang, Hao Tan, Jason Kuen, Henghui Ding, et al. Lazydit: Lazy learning for the acceleration of diffusion transformers. In *AAAI*, 2025.
- [37] Yecheng Wu, Zhuoyang Zhang, Junyu Chen, Haotian Tang, Dacheng Li, Yunhao Fang, Ligeng Zhu, Enze Xie, Hongxu Yin, Li Yi, et al. Vila-u: a unified foundation model integrating visual understanding and generation. *arXiv preprint arXiv:2409.04429*, 2024.
- [38] Ji Lin, Jiaming Tang, Haotian Tang, Shang Yang, Wei-Ming Chen, Wei-Chen Wang, Guangxuan Xiao, Xingyu Dang, Chuang Gan, and Song Han. Awq: Activation-aware weight quantization for llm compression and acceleration. In *MLSys*, 2024.
- [39] Xinyin Ma, Gongfan Fang, and Xinchao Wang. Llm-pruner: On the structural pruning of large language models. In *Advances in Neural Information Processing Systems*, 2023.
- [40] Xuan Shen, Peiyan Dong, Lei Lu, Zhenglun Kong, Zhengang Li, Ming Lin, Chao Wu, and Yanzhi Wang. Agile-quant: Activation-guided quantization for faster inference of llms on the edge. In *AAAI*, 2024.
- [41] Xuan Shen, Zhao Song, Yufa Zhou, Bo Chen, Jing Liu, Ruiyi Zhang, Ryan A. Rossi, Hao Tan, Tong Yu, Xiang Chen, Yufan Zhou, Tong Sun, Pu Zhao, Yanzhi Wang, and Jiuxiang Gu. Numerical pruning for efficient autoregressive models. *Proceedings of the AAAI Conference on Artificial Intelligence*, 39(19):20418–20426, Apr. 2025.
- [42] Guangxuan Xiao, Ji Lin, Mickael Seznec, Hao Wu, Julien Demouth, and Song Han. SmoothQuant: Accurate and efficient post-training quantization for large language models. In *Proceedings of the 40th International Conference on Machine Learning*, 2023.
- [43] Guangxuan Xiao, Yuandong Tian, Beidi Chen, Song Han, and Mike Lewis. Efficient streaming language models with attention sinks. *arXiv*, 2023.
- [44] Isaac Rehg. Kv-compress: Paged kv-cache compression with variable compression rates per attention head, 2024.

- [45] Coleman Hooper, Sehoon Kim, Hiva Mohammadzadeh, Michael W Mahoney, Yakun Sophia Shao, Kurt Keutzer, and Amir Gholami. Kvquant: Towards 10 million context length llm inference with kv cache quantization. *arXiv preprint arXiv:2401.18079*, 2024.
- [46] Akide Liu, Jing Liu, Zizheng Pan, Yefei He, Gholamreza Haffari, and Bohan Zhuang. Mini-cache: Kv cache compression in depth dimension for large language models. *arXiv preprint arXiv:2405.14366*, 2024.
- [47] Suyu Ge, Yunan Zhang, Liyuan Liu, Minjia Zhang, Jiawei Han, and Jianfeng Gao. Model tells you what to discard: Adaptive KV cache compression for LLMs. In *The Twelfth International Conference on Learning Representations*, 2024.
- [48] Yuhong Li, Yingbing Huang, Bowen Yang, Bharat Venkitesh, Acyr Locatelli, Hanchen Ye, Tianle Cai, Patrick Lewis, and Deming Chen. SnapKV: LLM knows what you are looking for before generation. In *The Thirty-eighth Annual Conference on Neural Information Processing Systems*, 2024.
- [49] Benjamin Spector and Chris Re. Accelerating llm inference with staged speculative decoding. *arXiv preprint arXiv:2308.04623*, 2023.
- [50] Nan Yang, Tao Ge, Liang Wang, Binxing Jiao, Daxin Jiang, Linjun Yang, Rangan Majumder, and Furu Wei. Inference with reference: Lossless acceleration of large language models. *arXiv preprint arXiv:2304.04487*, 2023.
- [51] Xupeng Miao, Gabriele Oliaro, Zhihao Zhang, Xinhao Cheng, Zeyu Wang, Zhengxin Zhang, Rae Ying Yee Wong, Alan Zhu, Lijie Yang, Xiaoxiang Shi, et al. Specinfer: Accelerating generative large language model serving with tree-based speculative inference and verification. *arXiv preprint arXiv:2305.09781*, 2023.
- [52] Xuefei Ning, Zinan Lin, Zixuan Zhou, Zifu Wang, Huazhong Yang, and Yu Wang. Skeleton-of-thought: Prompting LLMs for efficient parallel generation. In *The Twelfth International Conference on Learning Representations*, 2024.
- [53] Coleman Hooper, Sehoon Kim, Hiva Mohammadzadeh, Hasan Genc, Kurt Keutzer, Amir Gholami, and Sophia Shao. Speed: Speculative pipelined execution for efficient decoding. *arXiv preprint arXiv:2310.12072*, 2023.
- [54] Yao Teng, Han Shi, Xian Liu, Xuefei Ning, Guohao Dai, Yu Wang, Zhenguo Li, and Xihui Liu. Accelerating auto-regressive text-to-image generation with training-free speculative jacob decoding. *arXiv preprint arXiv:2410.01699*, 2024.
- [55] Hugo Touvron, Louis Martin, Kevin Stone, Peter Albert, Amjad Almahairi, Yasmine Babaei, Nikolay Bashlykov, Soumya Batra, Prajjwal Bhargava, Shruti Bhosale, et al. Llama 2: Open foundation and fine-tuned chat models. *arXiv preprint arXiv:2307.09288*, 2023.
- [56] Doyup Lee, Chiheon Kim, Saehoon Kim, Minsu Cho, and Wook-Shin Han. Autoregressive image generation using residual quantization. In *Proceedings of the IEEE/CVF Conference on Computer Vision and Pattern Recognition*, pages 11523–11532, 2022.
- [57] Ziqi Huang, Yinan He, Jiashuo Yu, Fan Zhang, Chenyang Si, Yuming Jiang, Yuanhan Zhang, Tianxing Wu, Qingyang Jin, Nattapol Chanpaisit, Yaohui Wang, Xinyuan Chen, Limin Wang, Dahua Lin, Yu Qiao, and Ziwei Liu. VBench: Comprehensive benchmark suite for video generative models. In *Proceedings of the IEEE/CVF Conference on Computer Vision and Pattern Recognition*, 2024.
- [58] Richard Zhang, Phillip Isola, Alexei A Efros, Eli Shechtman, and Oliver Wang. The unreasonable effectiveness of deep features as a perceptual metric. In *CVPR*, 2018.
- [59] Jonathan Ho and Tim Salimans. Classifier-free diffusion guidance. *arXiv preprint arXiv:2207.12598*, 2022.

Appendix

8 Additional Results

8.1 Detailed Results for VBench

We provide the detailed scores of VBench in Table 3 and Table 4. Our method better maintains the generation quality than SA methods. Specifically, on the VBench, when increasing the sparsity, unlike SA method with a significant drop on most of subtasks, our method keeps high scores close to the dense model on most subtasks under various sparsity.

Table 3: Detailed VBench scores.

Method	Replay Ratio	Local Size	Overall Consistency	Subject Consistency	Background Consistency	Temporal Flickering	Motion Smoothness	Dynamic Degree	Aesthetic Quality	Imaging Quality
Dense	/	/	27.9%	87.8%	94.6%	95.8%	94.9%	59.4%	57.4%	58.8%
Sparse Attn.	/	16	28.0%	71.9%	88.0%	84.5%	84.8%	100.0%	54.2%	59.1%
	/	32	27.9%	66.8%	86.2%	82.5%	82.3%	100.0%	54.2%	59.0%
	/	64	27.7%	67.4%	86.3%	84.6%	84.4%	100.0%	54.0%	58.0%
	/	128	27.5%	63.7%	85.1%	84.4%	84.3%	99.7%	52.9%	57.2%
	/	256	27.8%	82.7%	92.8%	92.5%	92.4%	94.4%	55.9%	56.8%
Ours	10%	/	27.7%	86.2%	94.0%	95.9%	94.6%	57.8%	57.0%	57.5%
	20%	/	27.9%	86.7%	93.7%	95.5%	94.7%	57.5%	56.9%	57.4%
	30%	/	27.9%	85.7%	93.4%	95.1%	94.4%	52.8%	57.0%	57.1%
	40%	/	27.9%	87.1%	93.7%	95.0%	94.9%	35.6%	57.2%	57.5%
	50%	/	27.9%	88.2%	94.1%	95.1%	95.0%	20.6%	57.7%	57.8%
	60%	/	27.9%	89.3%	94.2%	94.9%	95.2%	12.8%	57.9%	58.0%
	70%	/	28.1%	89.4%	94.1%	94.4%	95.0%	11.4%	58.2%	58.3%
	80%	/	28.2%	88.7%	93.8%	93.7%	94.4%	23.3%	58.2%	58.5%

Table 4: Detailed VBench scores.

Method	Replay Ratio	Local Size	Object Class	Multiple Objects	Human Action	Color	Spatial Relationship	Scene	Appearance Style	Temporal Style
Dense	/	/	76.7%	30.8%	74.8%	82.0%	37.6%	42.6%	24.7%	25.0%
Sparse Attn.	/	16	67.8%	20.5%	81.8%	81.7%	41.2%	37.3%	24.6%	24.9%
	/	32	65.7%	19.0%	83.2%	80.0%	37.2%	35.0%	24.5%	24.8%
	/	64	61.9%	17.2%	81.8%	77.6%	30.9%	33.7%	24.5%	25.2%
	/	128	50.1%	12.0%	78.8%	73.4%	19.9%	32.6%	24.3%	25.1%
	/	256	68.1%	26.6%	80.4%	76.7%	31.8%	38.9%	24.5%	25.3%
Ours	10%	/	74.9%	33.7%	76.8%	78.6%	42.2%	40.4%	24.7%	24.9%
	20%	/	74.0%	34.0%	76.0%	78.9%	41.0%	40.6%	24.7%	25.1%
	30%	/	74.4%	32.8%	75.8%	78.0%	39.8%	40.8%	24.8%	25.1%
	40%	/	76.5%	31.0%	73.8%	76.1%	40.9%	40.6%	24.7%	25.2%
	50%	/	77.1%	34.3%	74.0%	76.8%	42.7%	42.0%	24.8%	25.2%
	60%	/	77.6%	36.0%	75.4%	79.2%	43.5%	42.2%	24.8%	25.3%
	70%	/	77.9%	36.3%	79.0%	79.2%	43.8%	42.6%	24.8%	25.3%
	80%	/	77.9%	36.3%	75.4%	77.3%	44.9%	42.3%	24.7%	25.4%

8.2 Detailed Ablation Results for Threshold Distribution

We provide full results for the ablation of threshold distribution in Table 5. We observe that consistent threshold achieves better performance with lower LPIPS and higher VBench score than inconsistent thresholds, which verifies the effectiveness of Remark 4.5 discussed in Section 4.4.

8.3 Detailed Ablation Results for Threshold Values

We provide full results for the ablation of threshold values in Table 6. When $\tau \leq -2.5$, if we continue to decrease τ , the generation quality does not further degrade while higher sparsity with faster inference is achieved, demonstrating the robustness of FastCar. Additionally, we observe that the AR video generation model achieves the highest replay ratio of 87% when $\tau \approx -8$, indicating that only 13% of the MLP modules are actually required during the generation process.

8.4 Full Results for Additional Analysis

We provide full results for the combination of the sparse attention method and our method in Table 7. The results show that our method significantly boosts the performance of SA method through the straightforward combination. This validates the effectiveness of our method as a complementary enhancement to existing SA approaches.

Table 5: Full results for the ablation of the threshold distribution.

Threshold Distribution	Replay Ratio	PSNR ↑	SSIM ↑	LPIPS ↓	VBench Score		
					Total	Quality	Semantic
Consistent	10%	18.57	53.32	27.31	73.4%	75.5%	65.2%
Inconsistent	10%	16.73	46.63	32.94	71.8%	73.7%	64.3%
Consistent	20%	17.94	51.01	27.57	73.2%	75.3%	65.1%
Inconsistent	20%	16.30	45.05	33.60	71.7%	73.3%	65.4%
Consistent	30%	17.87	50.29	28.02	72.4%	74.3%	64.7%
Inconsistent	30%	16.67	45.39	31.96	72.5%	74.0%	66.5%
Consistent	40%	17.68	50.14	28.15	71.8%	73.0%	67.2%
Inconsistent	40%	17.34	48.61	30.65	71.8%	73.6%	64.5%
Consistent	50%	17.85	50.11	28.08	71.5%	72.7%	66.6%
Inconsistent	50%	17.65	49.94	29.40	71.5%	73.0%	65.4%
Consistent	60%	17.85	50.55	28.72	71.4%	72.7%	66.2%
Inconsistent	60%	17.79	49.55	28.56	71.3%	72.5%	66.5%
Consistent	70%	17.86	50.18	28.79	71.2%	72.3%	66.9%
Inconsistent	70%	17.68	48.84	29.39	71.1%	72.4%	65.9%
Consistent	80%	17.71	49.01	29.50	71.5%	73.0%	65.6%
Inconsistent	80%	17.59	48.06	30.01	71.3%	72.5%	66.3%

Table 6: Full results for the ablation of the threshold values.

Threshold Values	Replay Ratio	PSNR ↑	SSIM ↑	LPIPS ↓	VBench Score		
					Total	Quality	Semantic
0	3.96%	19.71	57.66	24.14	73.7%	75.7%	65.8%
-0.5	9.13%	18.61	53.49	27.27	73.6%	75.6%	65.5%
-1	17.32%	17.84	50.49	29.22	73.0%	75.1%	64.6%
-1.5	27.81%	17.31	48.39	30.85	72.6%	74.5%	64.7%
-2	40.92%	17.38	48.84	30.45	71.9%	73.6%	65.2%
-2.5	54.55%	17.76	50.30	29.05	71.4%	72.7%	65.8%
-3	66.78%	17.87	50.42	28.69	71.3%	72.5%	66.3%
-3.5	76.20%	17.76	49.42	29.26	71.3%	72.6%	66.2%
-4	82.41%	17.65	48.51	29.83	71.4%	72.7%	66.2%
-8	87.49%	17.60	48.50	30.09	71.5%	72.9%	66.0%
-16	87.49%	17.60	48.04	30.09	71.5%	72.9%	66.0%

Table 7: Full results for the combination of the sparse attention method and our method.

Method	Threshold Value	Replay Ratio	Local Size	PSNR ↑	SSIM ↑	LPIPS ↓	VBench Score			TFLOPs ↓	Latency (s) ↓	Power Eff. ↑
							Total	Quality	Semantic			
Dense	/	/	/	-	-	-	74.1%	76.4%	65.0%	31.79	689.71	1.47
Ours + Sparse Attn.	-1	17.72%	16	12.96	29.57	55.13	60.8%	61.6%	57.8%	28.05	497.35	2.03
	-2	46.11%	16	14.38	36.14	47.50	64.7%	66.5%	57.5%	23.69	427.75	2.36
	-3	70.23%	16	16.95	45.72	34.25	70.5%	72.0%	64.9%	19.81	356.35	2.84
	-4	83.85%	16	17.27	46.49	32.37	71.6%	73.1%	65.7%	17.87	331.29	3.05
Ours + Sparse Attn.	-1	17.72%	32	13.25	31.58	53.77	61.2%	61.9%	58.2%	28.07	499.79	2.02
	-2	46.11%	32	14.43	36.81	47.18	65.0%	66.6%	59.0%	23.71	430.18	2.35
	-3	70.23%	32	16.94	46.02	34.09	70.8%	72.3%	64.9%	19.83	358.78	2.82
	-4	83.85%	32	17.27	46.75	31.96	71.9%	73.4%	65.9%	17.89	333.73	3.03
Ours + Sparse Attn.	-1	17.72%	64	13.25	31.90	54.32	60.0%	60.9%	56.5%	28.10	504.60	2.00
	-2	46.11%	64	14.41	36.83	47.72	64.6%	66.2%	58.4%	23.74	435.00	2.33
	-3	70.23%	64	16.88	45.87	34.60	70.4%	71.8%	64.7%	19.86	363.60	2.78
	-4	83.85%	64	17.27	46.70	32.09	71.6%	73.1%	65.5%	17.92	338.55	2.99
Ours + Sparse Attn.	-1	17.72%	128	13.14	31.63	55.02	59.1%	60.3%	53.9%	28.16	514.00	1.97
	-2	46.11%	128	14.44	37.20	47.80	64.2%	65.9%	57.6%	23.80	444.40	2.28
	-3	70.23%	128	16.89	46.02	34.77	70.0%	71.5%	63.9%	19.92	373.00	2.71
	-4	83.85%	128	17.29	46.79	32.10	71.7%	73.3%	65.7%	17.98	347.95	2.91
Ours + Sparse Attn.	-1	17.72%	256	15.22	40.77	44.61	67.7%	70.0%	58.7%	28.28	531.87	1.90
	-2	46.11%	256	15.78	43.05	40.25	68.9%	71.1%	60.1%	23.92	462.27	2.19
	-3	70.23%	256	17.21	47.63	32.94	70.7%	72.2%	64.8%	20.04	390.87	2.59
	-4	83.85%	256	17.44	47.57	31.27	71.8%	73.3%	65.7%	18.10	365.82	2.76

9 Additional Visualization

We visualize the results of our method under different replay ratios. Our method generates high quality videos.

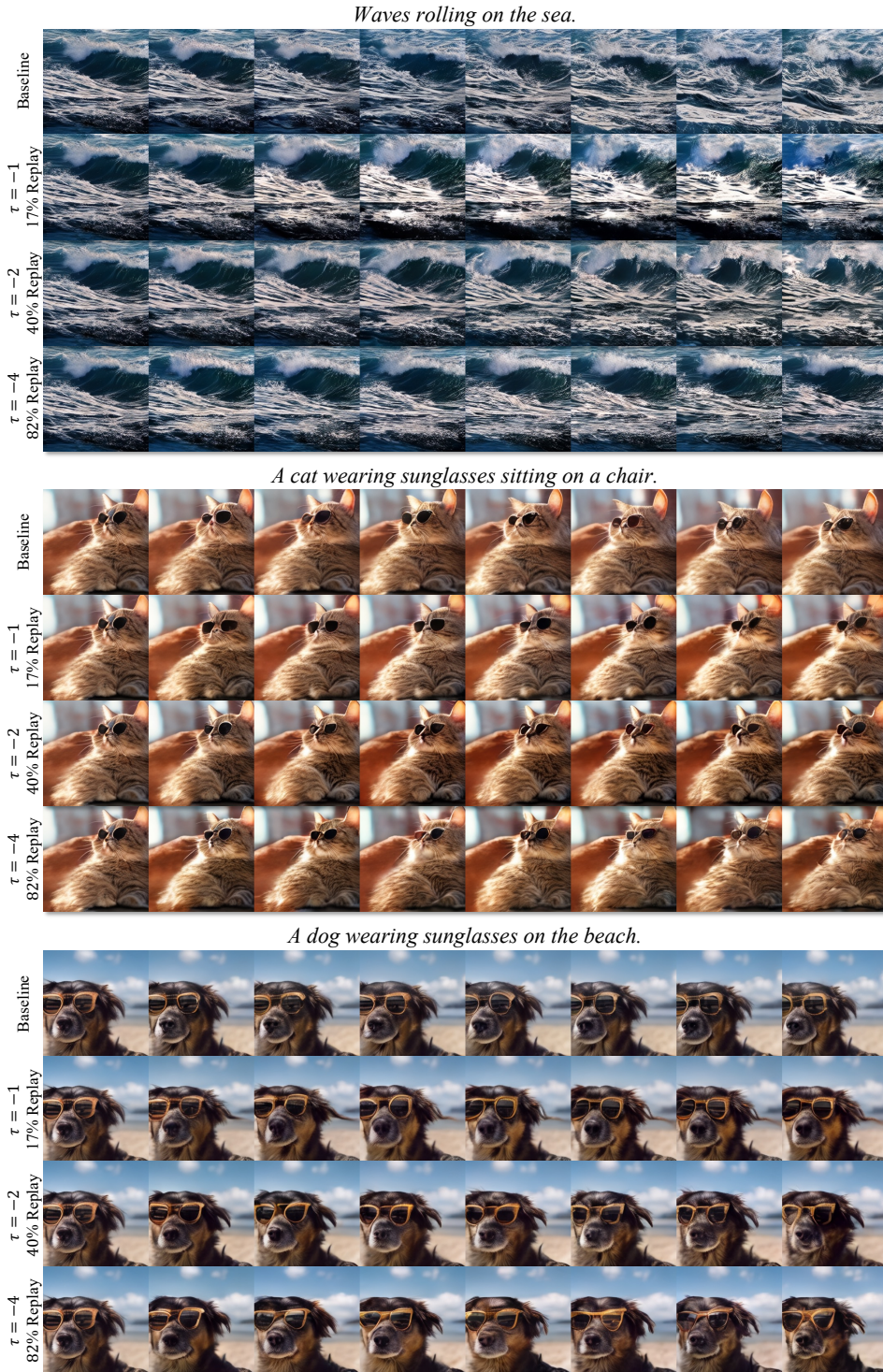


Figure 7: Additional visualization with threshold $\tau = -1, -2, -4$.

10 Detailed Proofs

10.1 Proof of Theorem 4.4

Proof of Theorem 4.4. Step 1 (Score exactly matches cosine similarity). By Definition 4.3, $s_{t,i} = \langle q_j, k_{j-} \rangle / \sqrt{d}$, where $q_j = x_j W_Q$ and $k_{j-} = x_{j-} W_K$. Under Assumption (3), $\|q_j\|_2 = \|k_{j-}\|_2 = 1$, so $s_{t,i}$ (up to \sqrt{d} scaling) equals the cosine similarity:

$$\cos \theta(q_j, k_{j-}) = \langle q_j, k_{j-} \rangle.$$

Thus, by the Law of Cosines for unit vectors,

$$\|q_j - k_{j-}\|_2^2 = 2(1 - s_{t,i}).$$

Step 2 (Logit gap from query gap). The attention logits satisfy

$$\ell_j = q_j K^\top, \quad \ell_{j-} = q_{j-} K^\top,$$

thus

$$\begin{aligned} \|\ell_j - \ell_{j-}\|_2 &= \|(q_j - q_{j-})K^\top\|_2 \\ &\leq \|K\|_2 \|q_j - q_{j-}\|_2, \end{aligned}$$

where $K = XW_K$ is the stacked key matrix. Since $K = XW_K$, we have

$$\|K\|_2 \leq \|X\|_2 \|W_K\|_2 \leq \sqrt{n}M\Lambda,$$

where $\|X\|_2 \leq \sqrt{n}M$ since each $\|x_j\|_2 \leq M$.

Step 3 (Attention output is Lipschitz). Since softmax and value projection are Lipschitz continuous (see [36]), there exists $L_{\text{attn}} > 0$ such that

$$\|\text{Attn}(X)_{j,:} - \text{Attn}(X)_{j-, :}\|_2 \leq L_{\text{attn}} \|\ell_j - \ell_{j-}\|_2 \leq C_1 \|q_j - q_{j-}\|_2,$$

where $C_1 = L_{\text{attn}} \sqrt{n}M\Lambda$.

Step 4 (Bounding query-key difference). Since

$$q_{j-} = x_{j-} W_Q, \quad k_{j-} = x_{j-} W_K,$$

it follows that

$$\|k_{j-} - q_{j-}\|_2 = \|x_{j-} (W_K - W_Q)\|_2 \leq \gamma \|x_{j-}\|_2 \leq \gamma M.$$

By triangle inequality,

$$\|q_j - q_{j-}\|_2 \leq \|q_j - k_{j-}\|_2 + \|k_{j-} - q_{j-}\|_2 \leq \sqrt{2(1 - s_{t,i})} + \gamma M.$$

Step 5 (Final bound). Thus,

$$\begin{aligned} \|\text{Attn}(X)_{j,:} - \text{Attn}(X)_{j-, :}\|_2 &\leq C_1 \left(\sqrt{2(1 - s_{t,i})} + \gamma M \right) \\ &\leq C \left(\sqrt{1 - s_{t,i}} + \gamma M \right), \end{aligned}$$

after absorbing constants into $C > 0$. This completes the proof. \square

10.2 Proof of Theorem 4.6

Proof of Theorem 4.6. Define

$$Z_j = \text{Attn}(X)_{j,:} + X_{j,:}, \quad Z_{j-} = \text{Attn}(X)_{j-, :} + X_{j-, :}.$$

Then

$$Y_{j,:} = \text{MLP}(Z_j), \quad Y_{j-, :} = \text{MLP}(Z_{j-}).$$

By Lipschitz continuity of MLP,

$$\|Y_{j,:} - Y_{j-, :}\|_2 \leq L \|Z_j - Z_{j-}\|_2.$$

Expanding $Z_j - Z_{j-}$ and applying triangle inequality,

$$\|Z_j - Z_{j-}\|_2 \leq \|\text{Attn}(X)_{j,:} - \text{Attn}(X)_{j-, :}\|_2 + \|X_{j,:} - X_{j-, :}\|_2.$$

The claim follows. \square

10.3 Proof of Theorem 4.7

Proof of Theorem 4.7. By Theorem 4.6,

$$\|Y_{j,:} - Y_{j-,:}\|_2 \leq L (\|X_{j,:} - X_{j-,:}\|_2 + \|\text{Attn}(X)_{j,:} - \text{Attn}(X)_{j-,:}\|_2) .$$

By Theorem 4.4,

$$\|\text{Attn}(X)_{j,:} - \text{Attn}(X)_{j-,:}\|_2 \leq C' (\sqrt{1 - s_{t,i}} + \gamma M) .$$

Substituting gives

$$\|Y_{j,:} - Y_{j-,:}\|_2 \leq C (\|X_{j,:} - X_{j-,:}\|_2 + \sqrt{1 - s_{t,i}} + \gamma M) ,$$

where $C = L(1 + C')$ absorbs constants. □